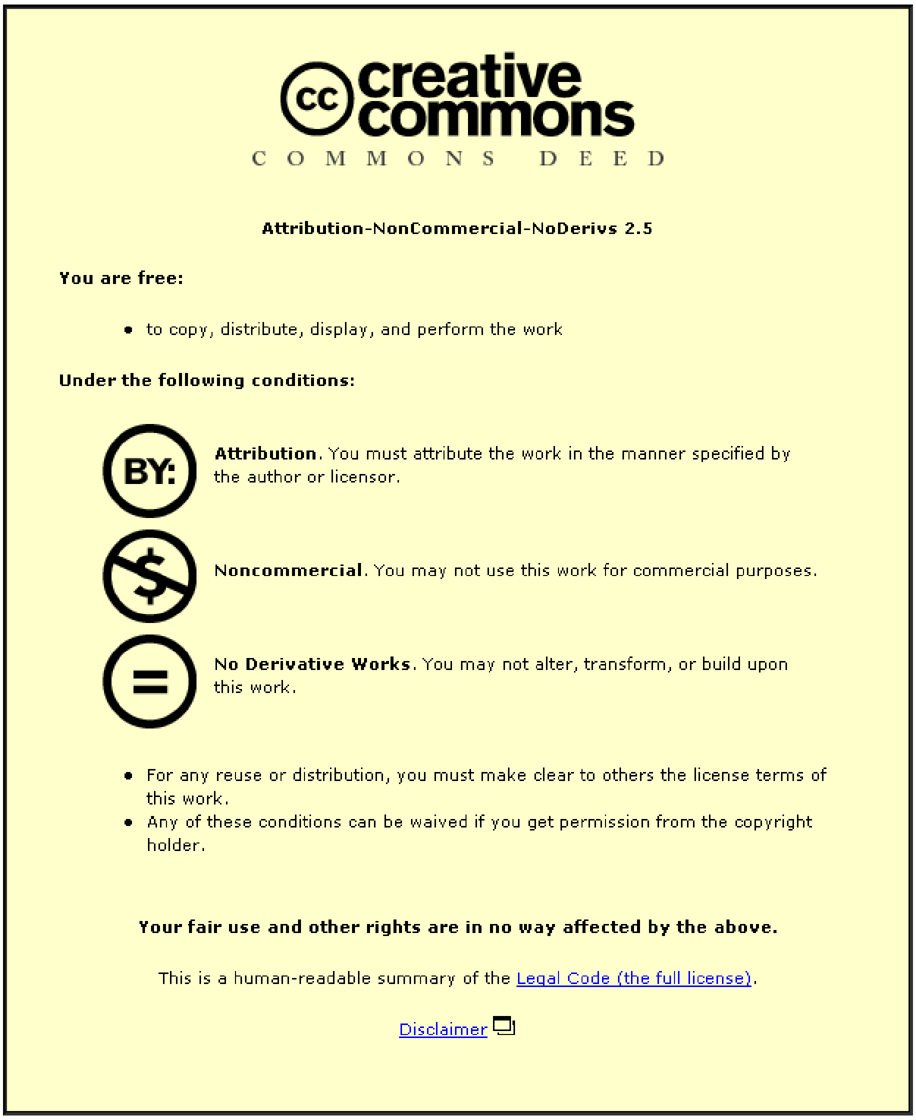

Investigation of the structure of ultra-thin films of Fe on Cu(111) using medium-energy ion scattering

M. D. Cropper*[1], T. C. Q. Noakes[2], M. T. Butterfield[1,3] and P. Bailey[2],

[1]*Department of Physics, Loughborough University, Loughborough, LE11 3TU, UK*

[2]*CLRC Daresbury Laboratory, Daresbury, Warrington, Cheshire, WA4 4AD, UK*

[3]*Present Address: Materials Science & Technology Division, Chemistry & Materials Science, Lawrence Livermore National Laboratory, P.O. Box 808, L-367, Livermore, CA 94550, USA*

The structure of a 12 ML ultra-thin film of Fe on Cu(111) has been investigated using medium-energy ion scattering. The as-deposited film was found to be poorly ordered with a mean square static displacement of 0.23 Å However, the order was improved by post-deposition annealing using temperatures up to 250°C, which reduced the mean square static displacement to 0.15 Å. The structure of the as-deposited film was consistent with a poorly ordered Kurjumov-Sachs coincidence - $(111)_{fcc}//(110)_{bcc}$, $[\bar{1}10]_{fcc}//[\bar{1}11]_{bcc}$, $[11\bar{2}]_{fcc}//[\bar{1}1\bar{2}]_{bcc}$ - as reported by other workers, but with some evidence of coexistence of other orientations. Upon annealing the more-ordered film structure was dominated by the Greninger-Troiano orientation – $(111)_{fcc}$~1° from $(110)_{bcc}$, $<112>_{fcc}$~2° from $[1\bar{1}0]_{bcc}$ - with coexistence of both Kurjumov-Sachs and Nishiyama-Wassermann - $(111)_{fcc}//(110)_{bcc}$, $[\bar{1}01]_{fcc}//[001]_{bcc}$, $[\bar{1}2\bar{1}]_{fcc}//[\bar{1}10]_{bcc}$ - coincidences.

Keywords: Iron; Fe; Copper; Cu(111); epitaxy; growth; orientational relationship; Kurjumav-Sachs; Greninger-Troiano; Nishiyama-Wassermann; MEIS; medium-energy ion scattering; disorder.

---

* Author to whom correspondence should be addressed.

INTRODUCTION

There is a large international activity in metal-on-metal epitaxy, motivated in part by the desire to produce metastable phases of magnetic transition metals. One element that can be produced in artificial structures with many interesting properties is iron. Iron is bcc at room temperature but the use of closely matched substrates has enabled the production of (fcc) γ-Fe, with a rich variety of magnetic properties, depending mainly upon the lattice spacing. The growth of γ-Fe has been studied on the (100) [1], (110) [2] and (111) [3-13] faces of Cu under a variety of conditions. Whilst the growth γ-Fe of on the (100) surface of Cu is well behaved, the growth on the closer packed (111) is much more complex.

The interest in Fe on Cu(111) has motivated several investigations of its structure. It has been studied by low energy electron diffraction (LEED) [3,4,5,6], angle-scanned photoelectron diffraction [5], energy-scanned photoelectron diffraction [7], scanning tunnelling microscopy (STM) [8,9,10,11], surface EXAFS [12] and normal incidence X-ray standing wave [13]. It is widely reported that Fe grows in a pseudomorphic fcc structure for the first few monolayer equivalents. Some LEED/AES investigations reported layer-by-layer growth [3,4], but angle-scanned photoelectron diffraction [5] and STM [10] measurements have shown that the Fe grows in 3-D islands and that the initial islands are mostly of bilayer height.

With increasing thickness, the Fe film relaxes to bcc, as determined by LEED [3], angle-scanned photoelectron diffraction [5], energy-scanned photoelectron diffraction [7] and surface EXAFS [12]. It is generally accepted that the bcc structure registers onto the fcc substrate with the Kurjumov-Sachs orientational relationship. This has the bcc (110) direction of the film normal to the surface and closely packed rows of atoms of both structures aligned. It is now thought that the transition begins between 2 and 4 ML, with a true bcc structure being present by about 5-8 ML. The angle-scanned photoelectron diffraction [5] and surface EXAFS [12] measurements indicated a transition region where neither fcc nor bcc was a good description, and that it was possible that domains of both were co-existing. The energy-scanned photoelectron diffraction [7] measurements, however, reported an abrupt transformation with the entire film converting to bcc. In contrast, STM images [10] show bright needle like areas that are considered to be needle like domains of bcc Fe sitting on fcc Fe.

The growth of a bcc(110) structure on an fcc surface plane is necessarily imperfect due to the difference in internal angle in the unit mesh. In the case of fcc(111) the internal angle is 120° whereas for bcc(110) it is 109.5°. This mismatch may lead to strain in the mesh resulting in a modification of the mesh shape and/or size. In particular, if in the KS orientation the closely packed bcc $[\bar{1}11]$ and fcc $[\bar{1}10]$ are aligned, then the open directions bcc $[\bar{1}10]$ and fcc $[\bar{2}11]$ must be out of alignment by, in principle, 5.3°. However, it is known that in the case of Fe on Cu(100) [1] small misalignments occur in the overlayer. To determine precise alignments in a system like Fe on Cu(1111) requires a method that is very precise in its measurement of angles. The imperfection of the matching of the film to the substrate is manifest in the LEED patterns reported, which have one-dimensional broadening of the spots indicating that there is a spread of alignments around the KS orientation.

Medium-energy ion scattering (MEIS) is a real space technique that allows the determination of surface and near-surface structures [14,15]. Surface crystallography may be determined by analysis of (incident) shadowing and (outgoing) blocking phenomena of elastically scattered ions, and by analysing the angular locations of the outgoing blocking dips at fixed incident directions. In addition to the elastic energy loss, inelastic processes reduce the energy of the ions by an amount proportional to path length through the surface region, enabling the depth of the scattering event to be determined. Thus MEIS is a structural technique with a depth resolution close to that of a single atomic layer thickness.

Despite the interest in the Fe on Cu(111) system, there have been few if any quantitative investigations into order and the influence of annealing on the structure. We have applied the method of MEIS to the study of Fe ultra-thin films deposited on Cu(111). The focus of the work has been on the degree of order in the films and the quantification of the orientational relationship between the bcc Fe overlayer and the fcc Cu substrate.

EXPERIMENTAL

The MEIS measurements were made using CLRC central facilities [16] based at Daresbury Laboratory, UK. A Cu(111) crystal was prepared ex situ using the usual methods. In situ sample preparation consisted of Ar^+ ion bombardment and annealing to produce a clean and well-ordered surface as judged by Auger electron spectroscopy (AES) and LEED. An iron film was deposited with the substrate close to room temperature (<50°C) using a small e-beam evaporator in which a wire feedstock was heated by electron bombardment from a hot filament. The Fe feedstock was maintained at a high positive potential so there was a possibility of Fe ions impinging on the substrate in addition to the neutral species, but any such ion current was below the limits of detection. The coverage of Fe was estimated by AES using the attenuation lengths of the Auger electrons in the film from the universal curve [17]. The values for the Cu 920 eV LMM transition and the Fe 651 eV LMM transition were employed to determine the film thickness to an accuracy of 0.5 ML using published sensitivity factors. In addition, the thickness was estimated by using ion energy loss to measure the depth of structural transitions beneath the surface. The latter method was found to give film thickness estimates 50% larger than AES, probably reflecting islanding in the film. The islands will have depths larger than those expected for the equivalent number of ML of a continuous film. Throughout this report, the quoted thickness of 12 ML must be regarded as monolayer equivalents and is the thickness as indicated by AES.

The MEIS system is equipped with a preparation chamber for sample cleaning and film evaporation, and a scattering chamber for the ion scattering experiments. The scattering chamber contains a rotatable toroidal sector ion energy analyser fitted with a two-dimensional position-sensitive detector that allows a range of ion energies and emission angles to be measured simultaneously. Adjusting the angular position and applied potentials can provide several 2-D ‘tiles’ that may be joined together to give a more complete coverage of both energy and angular parameters. After transfer of the sample to the scattering chamber, scattered ion intensity data were collected using 50 keV H^+ ions incident in the $[00\bar{1}]$ direction with the analyser in the plane of incidence. This energy of ion and experimental geometry was selected to maximise depth resolution at the expense of mass resolution. The data tiles were reduced to blocking curves (plots of scattered ion intensity from a specific range of depths as a function of scattering angle) using a polygon procedure to account for the variation of elastic energy loss with scattering angle and the effect of path length on inelastic energy loss. The polygons were used to isolate data corresponding to particular layers of the structure [18] estimated using stopping powers calculated by the SRIM code [19]. The effective depth resolution at a typical scattering angle when corrected for the path length imposed by the geometry was 0.86 Å at the surface, but which degrades with increasing depth owing to straggling. In this way, the scattering originating from the Fe overlayer and the Cu substrate could be separated despite their individual elastic scattering signals not being energetically resolved [18]. However, it should be borne in mind that the scattering from the Fe and Cu atoms will not be fully separated due to intermixing between film and substrate and the incomplete coverage due to islanding. The MEIS data were collected for the as-deposited film and following successive flash heating to 100°C, 150°C, 200°C and 250°C.

RESULTS AND DISCUSSION

MEIS has been used to investigate a film of iron on Cu(111) with a nominal depth of 12 ML. Blocking curves extracted using the method described above are shown in Fig. 1. The substrate scattering signal shown (Fig.1(f)) was obtained by integration over the energy range estimated to correspond to scattering from atoms in the Cu(111) substrate. For all the curves, the counts originating from the outermost layer have been subtracted, as this cannot produce blocking dips. The angular positions of the dips in the substrate scattering signal have been used to correct the angular scale of the data to within 0.5°, which is a standard procedure for this instrument [16]. The strong dip in this data range corresponds to the $[\bar{1}11]$ blocking direction that is expected to be at 54.8° scattering angle (70.5° exit angle).

Fig. 1 shows the scattering from the 12 ML film after a successive series of anneals. A feature of the blocking curves in Fig. 1 is the degree of order: The curves from the as-deposited film and those subjected to a low temperature anneal are representative of a structure that is poorly ordered, with blocking dips much weaker than those that would be obtained by simulation of the perfect structure. Clearly, the annealing improves the order of the film, the evidence being the increase in the relative depth of the blocking dips. Although the use of higher temperatures in growth produces a more ordered film, it does have a potential downside. In this case, elevated temperatures are likely to increase interdiffusion between Fe and Cu, similar to the surface segregation of Cu seen in Fe on Cu(100) [20]. It is clear from the blocking curves that if such interdiffusion is occurring it is not resulting in a Cu stabilised fcc Fe structure as has been reported for other Fe rich structures [21]. Quite the converse occurs, with a structure that clearly departs from fcc being formed.

A 12 ML film is well into the thickness regime where the film will have relaxed into bcc, so the blocking curves shown should be representative of the bcc structure. That the film differs from the substrate can be seen by comparing the curves for the iron with that from the substrate. The dip at 54.8° scattering angle in the substrate curve is due to the fcc $[\bar{1}11]$ direction. This is missing in the well-ordered films, but there are two new strong features at slightly smaller scattering angle and another at around 62°. Whilst comparisons with previous work might lead one to the assumption that the change in blocking features is associated with the transformation to bcc(110), the origin of the new blocking features in the 12 ML blocking curves are not obvious.

It has been widely reported that the Fe(110) film on Cu(111) can be described by the Kurjumov-Sachs (KS) orientational relationship. This is pictured schematically in Fig. 2. The Cu(111) surface has two major azimuthal directions, the close-packed [110] type directions and the less densely packed [211] type directions. For this experiment, the MEIS scattering plane is defined by the [111] surface normal and the $[\bar{2}11]$ azimuth. In the KS orientation, the closely packed $[\bar{1}11]$ row of the bcc(110) aligns with the closely packed $[\bar{1}01]$ row for the fcc(111). The three fold symmetry of the fcc(111) combined with the two fold symmetry of the bcc(110) produces six equivalent domains. The most common alternative orientational relationship is the Nishiyama-Wasserman (NW) in which the open bcc $[\bar{1}10]$ direction aligns with the fcc $[\bar{2}11]$. The angular difference between these two relationships is 5.26°. LEED studies of Fe on Cu(111) eliminate the NW as a possibility and there is general consensus that the structure aligns in the KS relationship, but with some distortion and disorder giving a spread of alignments.

To investigate the origin of the new blocking dips observed in the data, simulations were carried out using the VEGAS [22,23] code. Slabs of the bcc(110) structure were constructed and simulations generated for three incidence directions, as the effective number of domains is reduced from the original six by the symmetry of the measurement. The three domains were added together with an equal weight, though given the narrowness of the domains seen in STM images and the large angle of incidence it is possible that one or two domains will give a larger contribution to the blocking curve. Any such difference in weighting is likely to be small and the effect of varying the weights arbitrarily has been investigated and was found not to change the conclusions presented below. The simulations were carried out for misalignments between fcc $[\bar{2}11]$ and bcc $[\bar{1}10]$ from 0° (equivalent to NW) to 5.5° (close to KS) in 0.5° steps. These are shown in Fig. 3. From these curves it can clearly be seen that the well aligned undistorted KS is a poor description of the annealed structure with regards to ion scattering and that indeed if an ion scattering experiment had been the first to be performed on this system the structure may have been described as a distorted NW rather than KS. A simulation that shows qualitatively the main features of the data from the annealed films uses a misalignment of 2°. This, interestingly, is equivalent to the Greninger-Troiano [24] (GT) orientational relationship in which the bcc $[\bar{1}10]$ direction is ~2° from the fcc $[\bar{2}11]$ and there is a small misalignment of the two perpendicular axes such that the bcc [110] is ~1° from the fcc [111]. This is a fairly obscure relationship but it is occasionally seen in thin films. It is tempting to think that the GT may be the best description of the relationship, but the existence of this orientation alone has been ruled out in the as-deposited film by other workers using LEED. Note that when using these relationships, surface scientists should be wary as they are primarily used to describe the orientation of microscopic crystallites. However, perhaps what we are seeing on the nanometre scale is the origin of these larger scale structures.

In LEED the distinction between NW and KS is clear-cut in that the former gives clusters of three spots around the first order substrate spot whilst the latter gives a cluster of five. For the GT orientation, there would be a cluster of six spots caused by the action of the mirror plane on the angularly displaced three basic spots. In the KS two of these spots superpose. LEED work on films deposited at room temperature published by other workers unequivocally reports five spots so the alignment between the bcc $[\bar{1}11]$ and the fcc $[\bar{1}01]$ is clear and KS is probably the best description. However, there is severe disorder in the LEED patterns with two of the spots forming an arc that could hide GT and NW spots and indicating a spread of local alignments, with a maximum misalignment of 4.5°; less than the usual KS angle.

To investigate the effect of annealing on disorder and the spread of orientation of the unit meshes it is necessary to do quantitative fits to the data. The VEGAS routine does not have a simple means of incorporating static disorder, but there are two possible ways of introducing similar effects into the simulation. The best way is to increase the parameter that describes thermal disorder, the root mean square displacement. When this parameter is increased, the main effect on the simulations is to reduce the depth of the blocking dips. This leads to a second way of introducing the effects of disorder into the simulations, to simply add a constant offset to the simulations to artificially reduce the depth of the dips. The disadvantage of this latter method is that it is difficult to extract quantitative information on disorder from it, but it has the great advantage that it hugely simplifies the fitting procedure in a complicated situation such as the one investigated here.

The first attempt at quantitatively fitting the data utilised the latter method of incorporating disorder. Each of the simulations shown in Fig. 3 was fitted to each of the datasets shown in Fig 1. but with a constant offset added and also allowing a fraction of fcc Fe and its twin to be present. The results of these fits are shown in Fig. 4. In this figure the abscissa is the angle from the NW alignment, that is the angle between the fcc$[\bar{2}11]$ and the bcc$[\bar{1}10]$ directions, while the ordinate is the Rχ factor that is used to qualitatively determine the quality of the fit in MEIS experiments [25]. The data from the as-deposited film is shown using filled squares, to which the best fit is obtained using an angle of around 4°, close to the distorted KS orientation found by other authors. As the temperature of annealing increases, the behaviour of the Rχ factor with angle changes markedly. By 200°C the angle of best fit is at 2°: equivalent to the GT orientation. At lower temperatures, there is some evidence of a gradual reorientation with the dip corresponding to the KS orientation in evidence until 150°C. The likely coexistence of more than one orientation is also in evidence in the two lower temperature curves as can be seen more clearly in the inset. In creating these fits, it was necessary to use more simulated disorder for the low temperature curves than for the higher temperature ones.

To extract quantitatively the amount of static disorder, we have simulated its effect by increasing the parameter that describes thermal disorder. The expected root mean square displacement of Fe atoms ($<u^2>^{½}$) due to thermal effects at room temperature is 0.07 Å [26]. We have carried out simulation for values of the parameter between 0.07 and 0.28 Å and fitted them to the data. The initial fitting described above indicated that there may be a coexistence of differing orientations, so to investigate this we have allowed a mix of all possible orientations between NW and KS and the possibility of small amounts of fcc and fcc twin Fe. Fig. 5 shows the distributions of the coefficients of each orientation for each data set. The corresponding values of $<u^2>^{½}$ that gave the lowest value for R_χ in each case are given in Table 1. The curves generated by the fits are shown superimposed on the data in Figure 1.

The degree of confidence that can be put in these fits was investigated by investigating the effect on $R\chi$ of fixing the coefficients used in the fits to values other than those obtained for the natural best fit. It was found that the uncertainty in the ordinate in Fig. 5 varied from ±6% for the 0° coefficient to ±3% for the coefficients at angles around 4.5°. The uncertainties in the abscissa – the uncertainty in the orientation angle - varied from ±0.5° at low angle to ±1.5° at high angle. Thus, the areas of the graph that may broadly be described as NW, GT and KS are delineated by broken lines.

From Figure 5 it can be seen that the data is best described by a mix of orientations. The coefficients shown in the figure can best be separated into three regions; between 0 and 1 degree is NW, between 1.5 and 2.5 degrees is GT and beyond that KS. The data are best fit by a mix of orientations, with particularly high confidence for the annealed films. The dip at around 62° cannot be explained by a pure KS and requires rotations of much less than the nominal value for the structure, to around 2° equivalent to the GT alignment.

Table 1 indicates that the as-deposited film is indeed very poorly ordered; the mean square displacement due to disorder is 0.21 Å. Even for the more highly ordered annealed films, this value falls only to 0.15 Å. It should be expected that films of low quality be produced by evaporation at room temperature, as this is a low energy technique that does not provide sufficient activation energy to enable the growing structure to order properly. In virtually all areas of film deposition, whether of semiconductor superlattices or metallurgical films it is recognised that energetic deposition produces a better microstructure. In the first example, this is provided by an elevated substrate temperature and in the latter by ion assistance.

Conclusions

MEIS has been used to investigate the structure of a 12 ML film of Fe on Cu(111). Blocking curves have shown that the as-deposited film is poorly ordered. The dips from this are not consistent with a structure that is purely of KS orientation, but it contains a majority fraction of KS with additional regions of NW and GT. Upon annealing, the degree of order increases with blocking dips becoming much more visible. However, the annealing causes the structure to order into an array of orientations dominated by areas with the GT orientational relationship coexisting with KS and NW orientations.

Acknowledgements

This work was supported by the EPSRC via allocation of MEIS time to MDC and a research studentship to MTB. The FOM Institute (Amsterdam) provided the VEGAS code and Paul Quinn (Warwick) supplied the user-friendly PC interface for this.

References

---

[1] See for example A. Biedermann, R. Tscheliessnig, M Schmid and P Varga, Physical Review Letters 87 (2001) 086103.

[2] See for example S Tacchi, F Bruno and G. Carlotti, Surface Science 507 (2002) 324.

[3] D. Tian, F. Jona and P. M. Marcus, Physical Review B 45 (1992) 11216.

[4] Y. Darici, J. Marcano, H. Min and P. A. Montano, Surface Science 195 (1988) 566.

[5] M. T. Kief and W. F. Egelhoff Jr., Physical Review B 47 (1993) 10785.

[6] G. Gubbiotti, L. Albini, g. Carlotti, S. Loreti, C. Minarini, and M. De Crescenzi, Surface Science 433-435 (1999) 680.

[7] A. Theobald, O. Schaff, C. J. Hirschmugl, V. Fernandez, K.-M. Schindler, M. Polcik and A. M. Bradshaw, Physical Review B 59 (1999) 2313.

[8] A. Brodde, K. Drepps, J. Binder, Ch. Lunau and H. Neddermeyer, Physical Review B 47 (1993) 6609.

[9] J. Shen, M. Klaua, P. Ohresser, H. Jenniches, J. Barthel, Ch. V. Mohan, and J. Kirschner, Physical Review B 56 (1997) 11134.

[10] P. Ohresser, J. Shen, J. Barthel, M. Zheng, Ch. V. Mohan, M. Klaua and J. Kirschner, Physical Review B 59 (1999) 3696.

[11] M. C. G. Passeggi Jr., J. E. Prieto, R. Miranda, and J. M. Gallego, Surface Science 462 (2000) 45.

[12] M. T. Butterfield and M. D. Crapper, Surface Science 454-456 (2000) 719.

---

[13] M T Butterfield and M D Crapper, Surface Science 522 (2003) 167.

[14] J. F. van der Veen, Surface Science Reports 5 (1985) 199.

[15] R. M. Tromp, in *Practical Surface Analysis (Second Edition) Volume 2: Ion and Neutral Spectroscopy*, edited by D. Briggs and M. P. Seah (Wiley, Chichester, 1992), p.577.

[16] P Bailey, T C Q Noakes, and D P Woodruff, Surface Science 426 (1999) 358.

[17] M P Seah and W A Dench, Surface and Interface Analysis 1 (1979) 2.

[18] M. T. Butterfield, M. D. Crapper, T. C. Q. Noakes, P. Bailey, G. J. Jackson and D. P. Woodruff, Physical Review B 62 (2000) 16984.

[19] SRIM code, J. F. Ziegler, IBM Yorktown Heights, October 1999.

[20] Th. Detzel, Progress in Surface Science 48 (1995) 275

[21] M. Higa and M. Yamamoto, Journal of Physics: Condensed Matter 13 (2001) 6359.

[22] R. M. Tromp and J. F. van der Veen, Surface Science 133 (1983) 159.

[23] J. F. Frenken, J. F. van der Veen and R. M. Tromp, Nucl. Instrum. Methods Phys. Res. B 17 (1986) 334.

[24] T. J. Headley and J. A. Brooks, Metallurgical and Materials transactions, 33A (2002) 5.

[25] D Brown, T C Q Noakes, D P Woodruff, P Bailey and Y Le Goaziou, Journal of Physics: Condensed Matter, 11 (1999) 1889

[26] A Zangwill, Physics at Surfaces (Cambridge University Press, Cambridge, 1988)

Tables

Table 1: The values of $<u^2>^{½}$ required to fit the data and the value that is due to static disorder.

Annealing temperature	Total $<u^2>^{½}$ (Å)	R_χ	Static $<u^2>^{½}$ (Å)
As deposited	0.24	6.7	0.23
100°C	0.21	4.1	0.20
150°C	0.20	7.1	0.17
200°C	0.17	17.1	0.15
250°C	0.17	14.8	0.15

Figure Captions

Figure 1: The effect of low temperature post-deposition annealing on the MEIS blocking curves. The circles represent the experimental data and the solid lines the best fits obtained by simulation as described in the text. The panels (a) to (e) successively show the data from the as-deposited film, and following annealing to 100°C, 150°C, 200°C and 250°C. Panel (f) shows data from the Cu(111) substrate.

Figure 2: Schematic diagrams of the fcc(111) and bcc(110) planes with potential alignment directions indicated.

Figure 3: VEGAS simulations of the blocking curves obtained for ion incidence in the $[\bar{1}00]$ direction for different angles of misalignment between the fcc $[\bar{2}11]$ and bcc $[\bar{1}10]$ directions. An exemplar experimental data set is shown for convenience, the broken lines show the angular position of the main blocking dips.

Figure 4: Plot of $R\chi$ versus angle away from NW orientation for different annealing temperatures of the 12 ML film.

Figure 5: A graph showing the best-fit distributions of orientations for the different annealing temperatures of a 12 ML film. The fraction of fcc structure found to be present is denoted by “f” and the fraction of its twin by “t”. The abscissa shows the fraction of a bcc(110) structure with its $[\bar{1}11]$ azimuth misaligned from the fcc(111) $[\bar{1}01]$ azimuth by an angle of n.n°

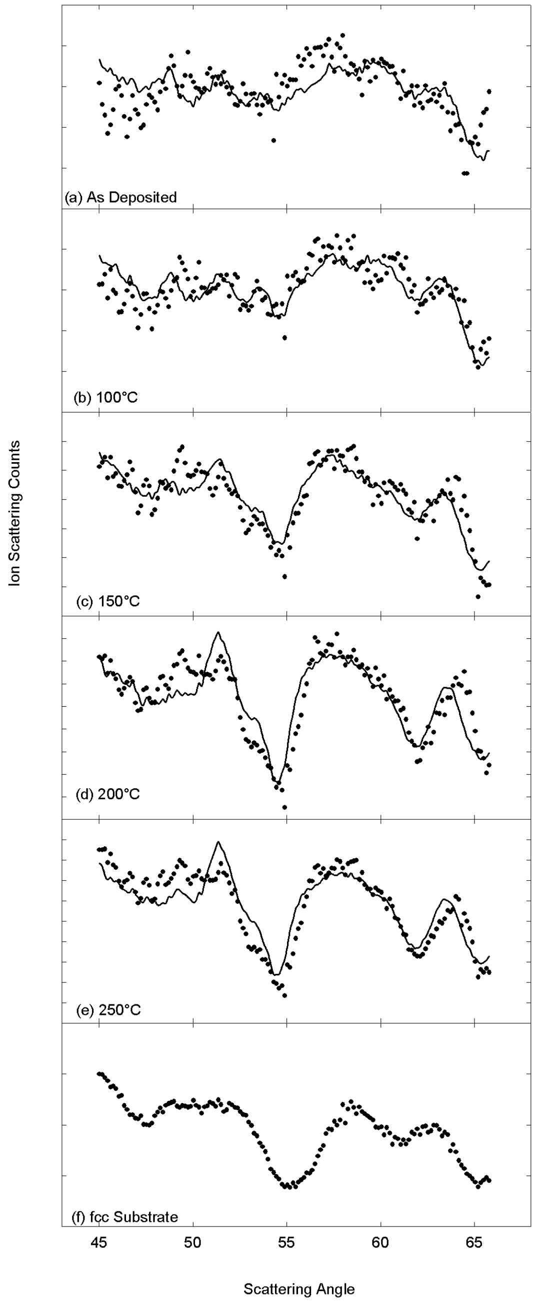
(a) As Deposited
(b) 100°C
(c) 150°C
(d) 200°C
(e) 250°C
(f) fcc Substrate
Ion Scattering Counts
45
50
55
60
65
Scattering Angle

.

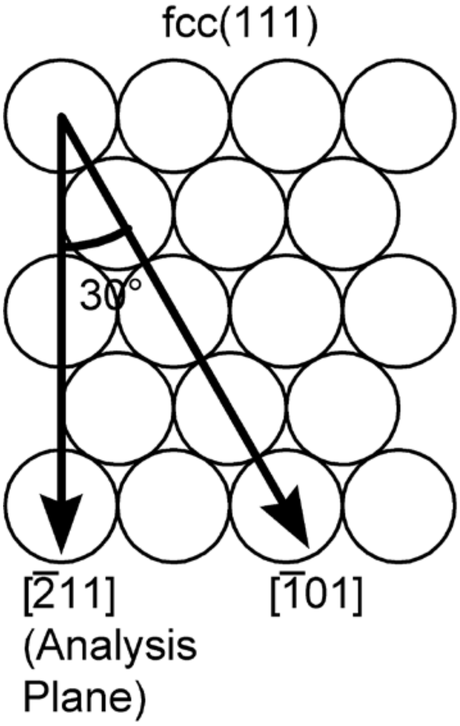
fcc(111)
30°
[$\bar{2}$11]
(Analysis Plane)
[$\bar{1}$01]

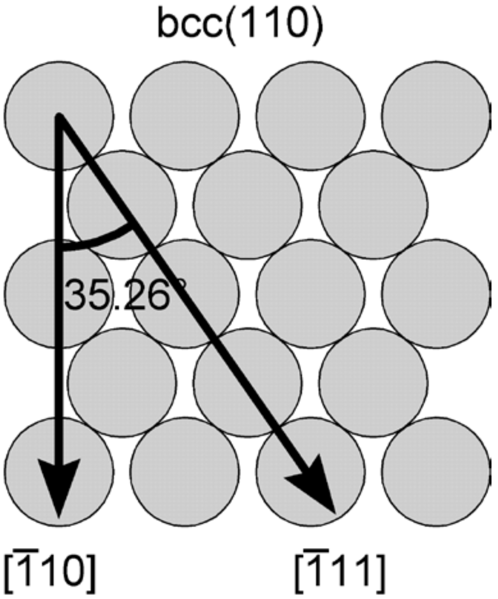
bcc(110)
35.26°
[$\bar{1}$10]
[$\bar{1}$11]

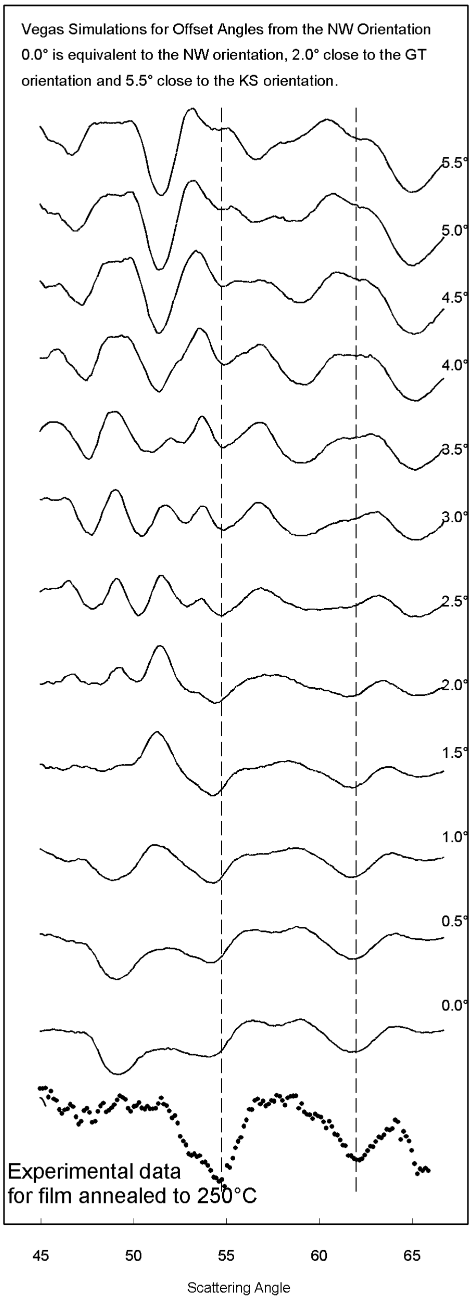

Vegas Simulations for Offset Angles from the NW Orientation
0.0° is equivalent to the NW orientation, 2.0° close to the GT orientation and 5.5° close to the KS orientation.

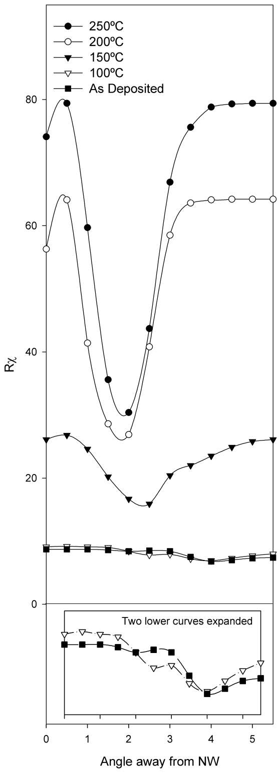
250ºC
200ºC
150ºC
100ºC
As Deposited
80
60
40
20
0
Rχ
Two lower curves expanded
0
1
2
3
4
5
Angle away from NW

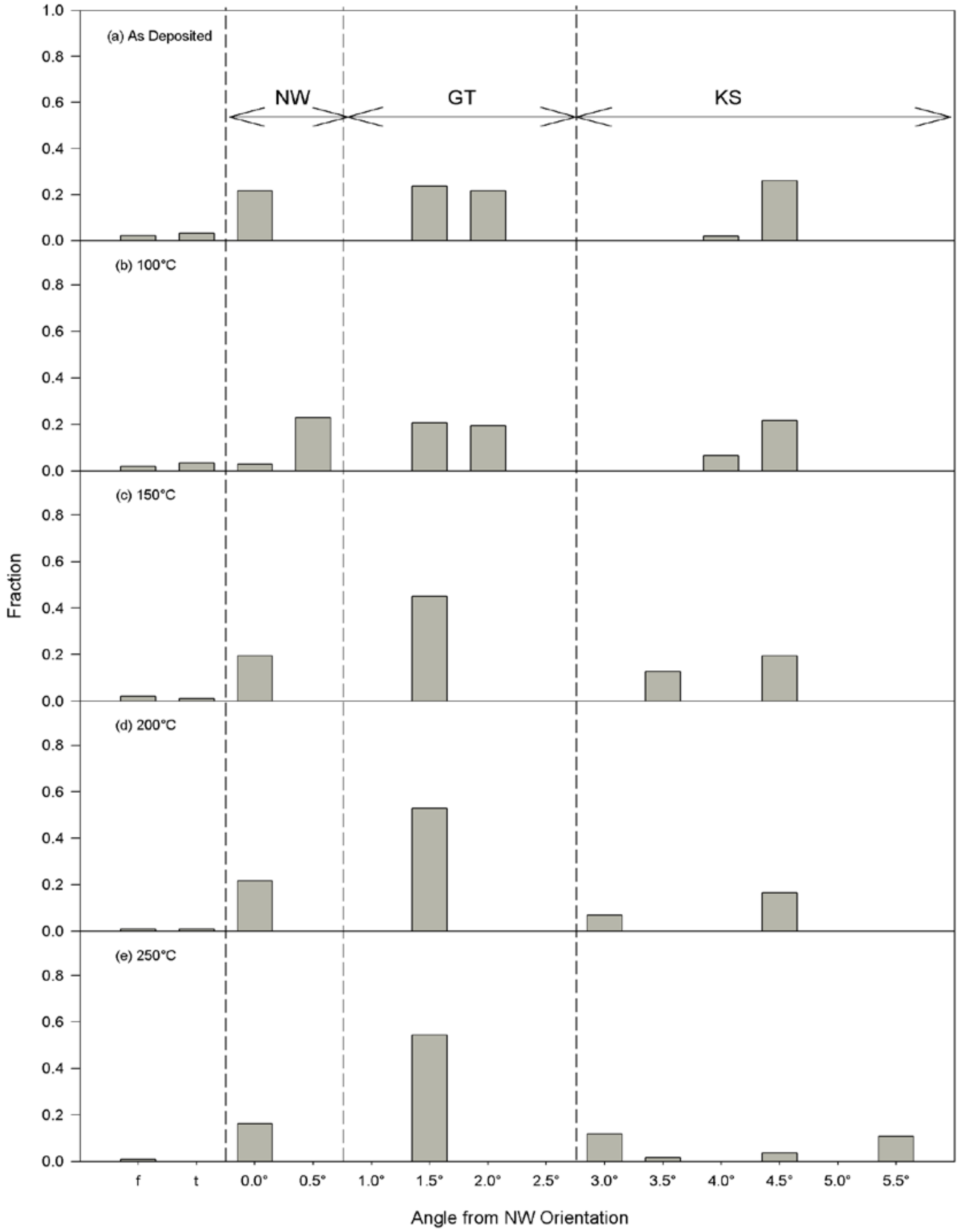
(a) As Deposited
NW
GT
KS
(b) 100°C
(c) 150°C
(d) 200°C
(e) 250°C
Fraction
1.0
0.8
0.6
0.4
0.2
0.0
f
t
0.0°
0.5°
1.0°
1.5°
2.0°
2.5°
3.0°
3.5°
4.0°
4.5°
5.0°
5.5°
Angle from NW Orientation